Journal of Sound and Vibration (2001) **245**(3), 562–570
doi:10.1006/jsvi.2000.3548, available online at http://www.idealibrary.com on IDEAL®

GEOMETRIC NONLINEAR EFFECT OF A TYPICAL CFRP PAYLOAD FAIRING ON DYNAMIC DISPLACEMENT RESPONSE

V. RAMAMURTI

Department of Applied Mechanics, Indian Institute of Technology, Madras 600 036, *India*

S. RAJARAJAN

Launch Vehicle Design Group, Vikram Sarabhai Space Centre, Trivandrum 695 022, *India*

AND

G. V. RAO

Structural Engineering Group, Vikram Sarabhai Space Centre, Trivandrum 695 022, *India.*
E-mail: gv_rao@vssc.org

(*Received* 22 *November* 2000)

1. INTRODUCTION

In space applications, large structures like payload fairing, etc. are subjected to severe transient loads which cause the structures to undergo large displacements. The payload fairing structure protects the spacecraft from adverse aerodynamic environments and this is separated after its purpose is served. The payload fairing structural configuration/test details of Atlas, Japanese H II and Titan 4 are discussed in references [1–3]. Many aspects of efficient payload fairing design are very well presented and the configurations are compared based on weight, cost and payload increments in reference [4]. Payload fairing is typically a thin stiffened shell type of structure and the large displacements constitute the class of geometric non-linear problems.

In the present work, the effect of geometric non-linearity of a typical CFRP payload fairing on dynamic displacement response due to a separation impulse is studied by a finite element method in conjunction with a mode superposition technique. A step-by-step analysis is performed on the deformed state of each previous time step.

2. STRUCTURAL DETAILS

The structural details and winding angle details of the CFRP payload fairing are given in Figure 1. This is basically a shell-type structure with number of stiffeners, bulk heads, end rings and edge beams. The structural properties of the beam members are given in Table 1.

0022-460X/01/330562 + 09 $35.00/0

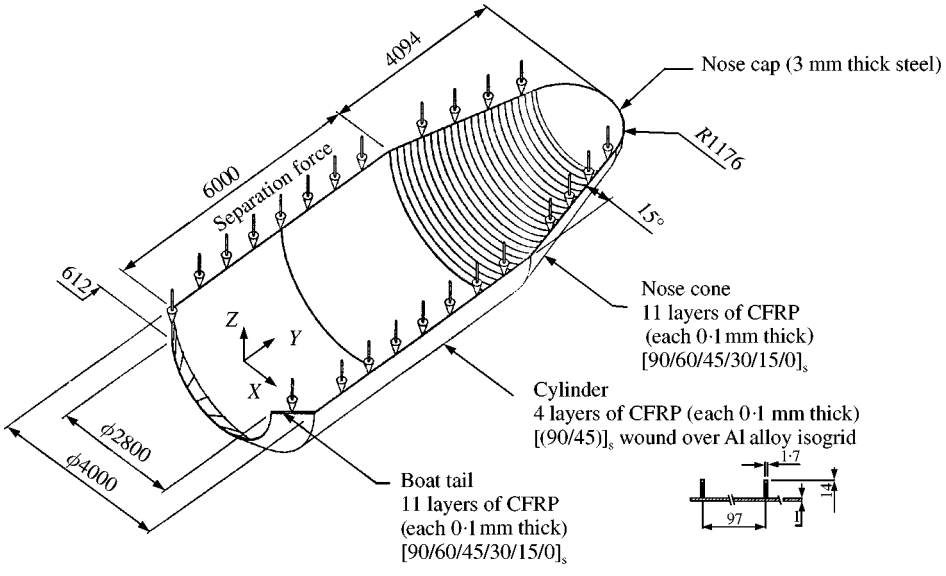

Figure 1. Typical CFRP payload fairing.

TABLE 1

Sectional properties of beam members

Description	Area (mm^2)	Moment of inertia (mm^4)		
		I_{xx}	I_{yy}	I_{zz}
Nose cone forward end ring	402	61 225	97 380	3565
Nose cone bulk head	128	11 166	33 333	119
Cylinder bulk head	757	238 782	128 553	10 390
Boat tail forward end ring	1108	371 131	272 033	25 065
Boat tail aft end ring	1212	664 364	160 271	41 483
Boat tail stiffeners	202	91 467	30 695	185
Nose cone aft end ring	895	293 014	136 454	12 606
Nose cap ring + nose cone forward end ring	718	201 436	155 217	5336
Piston beam	1362	279 300	955 800	6865
Nose cone edge beam	1289	469 824	608 174	3938
Boat tail edge beam	841	91 841	374 713	7959

3. FINITE ELEMENT FORMULATION

3.1. PLATE AND SHELL ELEMENT

Plate and shell finite elements are used for modelling boat tail, cylinder, nose cone and nose cap structural elements. This is a three-noded triangular element with six degrees of freedom per node namely, three axial displacements u, v, w and three rotations θ_x, θ_y, θ_z.

From the classical plate theory definitions, the force and moment resultants on a laminate are obtained by an integration of the stresses in each layer or lamina through the

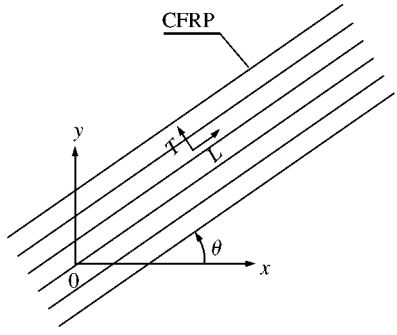

Figure 2. Fiber co-ordinate system. L–T is the longitudinal and transverse directions of fiber; θ is the fiber angle.

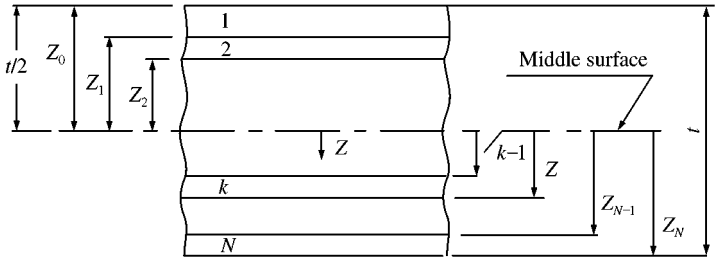

Figure 3. Nomenclature for the stacking sequence (N layers).

laminate thickness, t [5, 6]. The fiber co-ordinate system and the nomenclature for the stacking sequence are given in Figures 2 and 3 respectively. The elements of the material characterization matrices $[A]_{3\times3}$, $[B]_{3\times3}$, and $[D]_{3\times3}$ are given as

$$[A_{ij}] = \sum_{k=1}^{NLAY} [\bar{Q}_{ij}]_k (z_k - z_{k-1}), \tag{1}$$

$$[B_{ij}] = \frac{1}{2} \sum_{k=1}^{NLAY} [\bar{Q}_{ij}]_k (z_k^2 - z_{k-1}^2), \tag{2}$$

$$[D_{ij}] = \frac{1}{3} \sum_{k=1}^{NLAY} [\bar{Q}_{ij}]_k (z_k^3 - z_{k-1}^3). \tag{3}$$

The membrane and flexural nodal displacements are given as

$$\{\delta_p\} = [u_1\ v_1\ u_2\ v_2\ u_3\ v_3]^{\mathrm{T}}$$

$$\{\delta_f\} = [w_1\ \theta_{x1}\ \theta_{y1}\ w_2\ \theta_{x2}\ \theta_{y2}\ w_3\ \theta_{x3}\ \theta_{y3}]. \tag{4}$$

Linear polynomials in the area co-ordinates L_1, L_2, L_3 for membrane displacements u and v and cubic polynomials for flexural displacements w presented by Zienkiwicz [7] are used.

$$u = \beta_1 L_1 + \beta_2 L_2 + \beta_3 L_3,$$

$$v = \beta_4 L_1 + \beta_5 L_2 + \beta_6 L_3, \tag{5}$$

$$w = \alpha_1 L_1 + \alpha_2 L_2 + \alpha_3 L_3 + \alpha_4 (L_2^2 L_1 + \tfrac{1}{2} L_1 L_2 L_3) + \alpha_5 (L_1^2 L_2 + \tfrac{1}{2} L_1 L_2 L_3)$$

$$+ \alpha_6 (L_3^2 L_2 + \tfrac{1}{2} L_1 L_2 L_3) + \alpha_7 (L_2^2 L_3 + \tfrac{1}{2} L_1 L_2 L_3) + \alpha_8 (L_3^2 L_1 + \tfrac{1}{2} L_1 L_2 L_3)$$
$$+ \alpha_9 (L_1^2 L_3 + \tfrac{1}{2} L_1 L_2 L_3), \tag{6}$$

$$\{\varepsilon_p\} = \begin{Bmatrix} \varepsilon_x \\ \varepsilon_y \\ \gamma_{xy} \end{Bmatrix} = \begin{Bmatrix} \partial u/\partial x \\ \partial v/\partial y \\ \dfrac{\partial u}{\partial y} + \dfrac{\partial v}{\partial x} \end{Bmatrix} = [B_p]\{\delta_p\}, \tag{7}$$

$$\{\varepsilon_f\} = \begin{Bmatrix} -\partial^2 w/\partial x^2 \\ -\partial^2 w/\partial y^2 \\ -2\partial^2 w/\partial x \partial y \end{Bmatrix} = [B_f]\{\delta_f\}. \tag{8}$$

Substituting these into the energy expression

$$U = \frac{1}{2} \int_A \int [\{\varepsilon_p\}^{\mathrm{T}} [A] \{\varepsilon_p\} + \{\varepsilon_p\}^{\mathrm{T}} [B] \{\varepsilon_f\} + \{\varepsilon_f\}^{\mathrm{T}} [B] \{\varepsilon_p\} + \{\varepsilon_f\}^{\mathrm{T}} [D] \{\varepsilon_f\}] \, \mathrm{d}A, \tag{9}$$

the stiffness matrix consisting of the following submatrices for extensional, coupling and bending stiffnesses are obtained:

$$[k_{pp}] = \int_A \int [B_p]^{\mathrm{T}} [A] [B_p] \, \mathrm{d}A,$$

$$[k_{pf}] = \int_A \int [B_p]^{\mathrm{T}} [B] [B_f] \, \mathrm{d}A,$$

$$[k_{ff}] = \int_A \int [B_f]^{\mathrm{T}} [D] [B_f] \, \mathrm{d}A. \tag{10}$$

The consistent mass matrix is given by

$$[m] = \int_{vol} \rho [N]^{\mathrm{T}} [N] \, \mathrm{d}v, \tag{11}$$

where

$$[N] = \begin{bmatrix} [N_p] & 0 \\ 0 & [N_f] \end{bmatrix}. \tag{12}$$

This element is used for both orthotropic and isotropic layers of the shell structural elements. A typical finite element and the nodal degrees of freedom are shown in Figure 4.

3.2. 3-D BEAM ELEMENT

The stiffeners, end rings, edge beams, piston beams and bulk heads are modelled using a two-noded beam element with six degrees of freedom (Figure 5) with the following displacement vector:

$$\{\delta\} = [u_1 \; v_1 \; w_1 \; \phi_1 \; \varphi_1 \; \theta_1 \; u_2 \; v_2 \; w_2 \; \phi_2 \; \varphi_2 \; \theta_2]^{\mathrm{T}}. \tag{13}$$

As presented by Ramamurti [8], a linear variation has been assumed for the axial displacement and cubic polynomials for the lateral displacements.

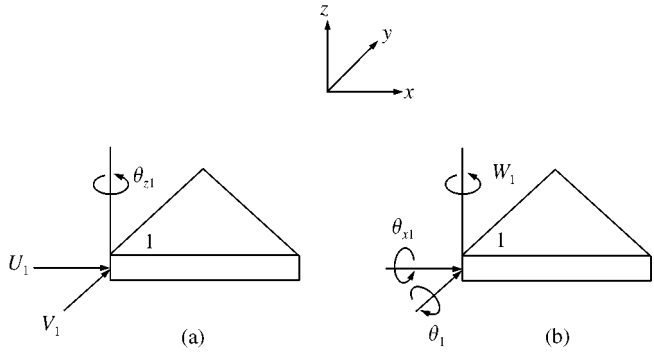

Figure 4. Three-noded plate and shell element. (a) In-plane displacement. (b) Bending displacement.

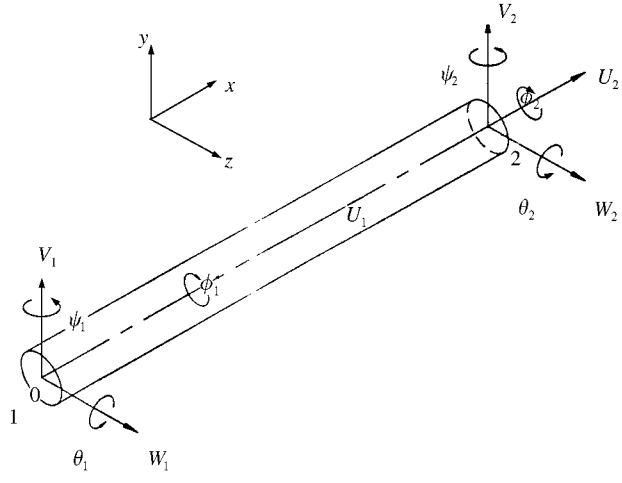

Figure 5. Two-noded 3-D beam element.

4. ANALYSIS

4.1. EIGENVALUE PROBLEM

The equation of motion of a free vibration problem is given by

$$[M]\{\ddot{\delta}\} + [K]\{\delta\} = 0. \tag{14}$$

Lanczos method in conjunction with an inverse iteration method is used to solve for the lowest eigenvalues and corresponding eigenvectors satisfying

$$[K]\{\delta\} = \omega^2[M]\{\delta\}, \tag{15}$$

where ω is the natural frequency of the structure.

4.2. RESPONSE ANALYSIS

For a system with damping the governing differential equation is given by

$$[M]\{\ddot{\delta}] + [C]\{\dot{\delta}\} + [K]\{\delta\} = \{f(t)\}. \tag{16}$$

1% damping is assumed for all the modes.

The mode superposition technique is used to de-couple the linear equations and solve for the displacement response.

4.3. INCREMENT METHOD

Though the increment method is used for static analysis, literature on the application of this technique with mode superposition is scarce. A separation force is acting for 5.0E-3 s and this time zone is divided into 10 equal time steps. A step-by-step eigenvalue and displacement response analysis are carried out. Each time step is further divided into smaller steps and the linear formulations described above are used for free vibration analysis and the mode superposition method is used to de-couple the equations and get the displacement histories. Before the loads corresponding to the next time step are applied, the finite element model is updated with the displacements at the beginning of this time step due to previously applied loads. Each time, the new geometry and the corresponding stiffness matrices are obtained and the analyses repeated. Utilizing the symmetry boundary condition, a half-model of the structure is idealized as shown in Figure 6. The displacement response in X (in the direction perpendicular to the direction of force application) and Z (along the direction of force application) directions due to the separation force given in Figure 7 are determined.

5. RESULTS AND DISCUSSIONS

The CFRP material properties used in the study are: $E_L = 0{\cdot}1302\text{E}6\,\text{N/mm}^2$, $E_T = 0{\cdot}6014\text{E}4\,\text{N/mm}^2$, $G_{LT} = 0{\cdot}2807\text{E}4\,\text{N/mm}^2$, $\mu_{LT} = 0{\cdot}314$ and $\rho = 1{\cdot}7\text{E-}9\,\text{Ns}^2/\text{mm}^4$. The first 25 modes are considered for the transient analysis. The displacement response history perpendicular to and along the force acting along directions at three important

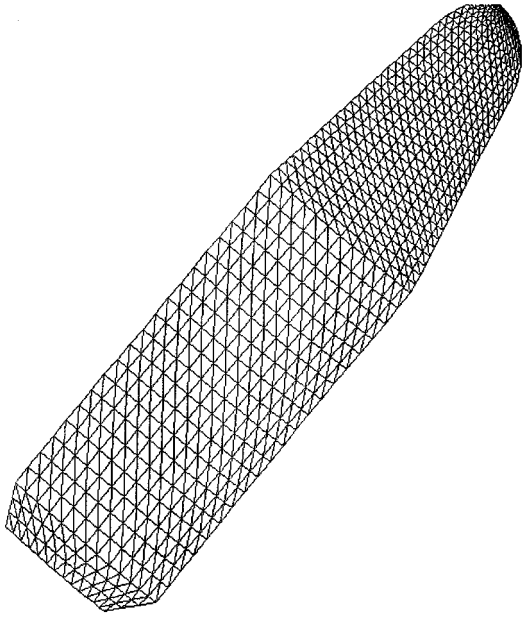

Figure 6. Finite element idealization. Total no. of elements: 1859, Total no. of nodes: 771.

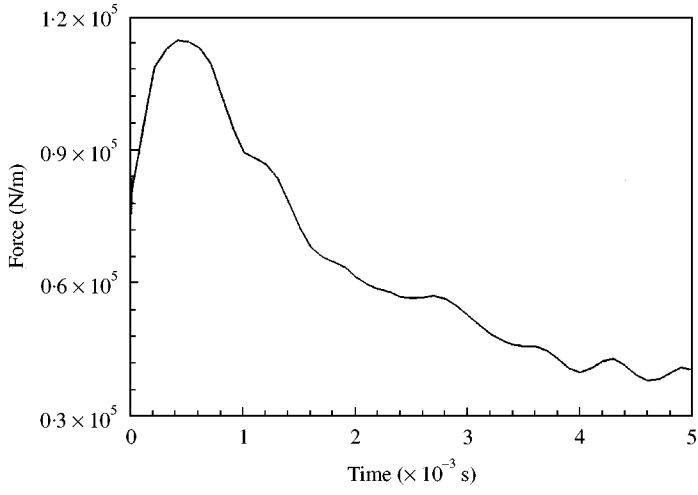

Figure 7. Typical separation impulse details.

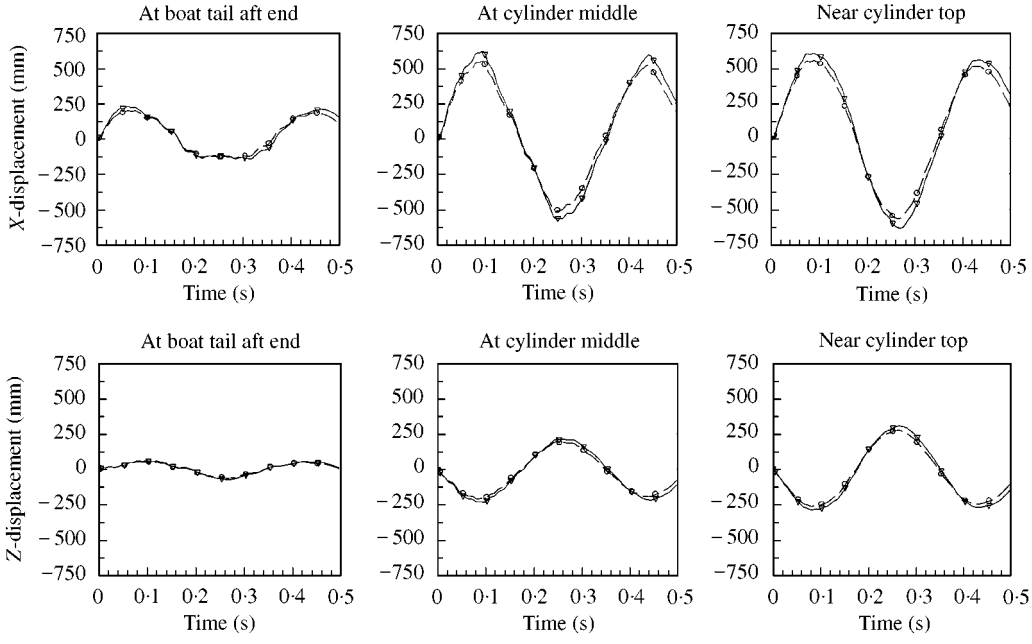

Figure 8. Comparative displacements in perpendicular (X direction) and along (Z direction) the force direction. ▽——▽, Linear analysis; ○——○, incremental technique.

locations namely the boat tail aft end, cylinder middle and near cylinder top are given in Figure 8. The displacements based on linear analysis are also included in this figure for comparison. The comparative peak displacement responses are given in Table 2. As can be seen, the stiffening effect is evident in both X and Z directions. The reduction in the displacement is to a maximum extent of about 13·6%. This is a significant observation and this is to be considered while studying the safe separation of the fairing.

TABLE 2

Peak displacements in one cycle

Location	*X* displacement (mm)		*Z* displacement (mm)	
	Present analysis	Linear analysis	Present analysis	Linear analysis
Boat tail aft end	200·2 − 132·9	229·6 − 138·1	55·6 − 64·6	60·5 − 74·8
Cylinder middle	548·3 − 514·0	618·9 − 565·8	− 208·5 194·0	− 231·2 210·4
Near cylinder top	546·3 − 569·0	597·8 − 635·1	− 266·5 274·7	− 291·6 305·8

6. CONCLUSION

The finite element method in conjunction with the mode superposition technique and incremental technique are used for studying the geometric non-linear effect of a typical CFRP payload fairing on the displacement response due to separation impulse. A step-by-step analysis is performed on the deformed state of the structure due to the load applied corresponding to the previous time step. A stiffening effect is observed and on account of this, there is a small increasing trend in the eigenvalues and a reduction in the displacement response. As the reduction in the displacement response is to a maximum extent of about 13·6%, the geometric non-linear effect has to be taken into account in all the related studies.

REFERENCES

1. F. SHEN and D. POPE 1991 *Aerospace Engineering* 19–22. Fairing structure for space launch vehicles.
2. M. J. ROBBINS 1990 *Research in Structures, Structural Dynamics and Materials, Long Beach, CA*, 194–205. NASA CP 3064. Ground test program for new Atlas payload fairing.
3. Y. YASUNAGA, Y. FUKUSHIMA, T. NAKAMURA and T. FUJITA 1990 *Proceedings of 28th Aerospace sciences meeting, Reno, Nevada*, 1–8. AIAA 90-0720. Separation jettison test of Japanese H-II rocket satellite fairing.
4. S. W. KANDEBO 1990 *Aviation Week & Space Technology* 58–62. Payload capacity of Titan 4 to expand with new fairing.
5. J. P. VINSON and R. L. SIERAKOWSKI 1987 *The Behaviour of Structures Composed of Composite Materials*. Dordrecht: Martinus Nijhoff Publishers.
6. R. M. JONES 1975 *Mechanics of Composite Materials*. New York: Hemisphere Publishing Corporation.
7. O. C. ZIENKIWICZ 1971 *The Finite Element Method in Engineering Science*. London: McGraw-Hill Publications; second edition.
8. V. RAMAMURTI 1996 *Computer Aided Mechanical Design and Analysis*. New Delhi: Tata McGraw-Hill Publishing Company; third edition.

APPENDIX A: NOMENCLATURE

A	area of the triangular element
$[A]$, $[B]$, $[D]$	material characterization matrix relating stress resultants and the strain of a laminate

$[B_p]$, $[B_f]$	membrane and flexural strain–displacement matrix
$[C]$	damping matrix
E_L, E_T	Young's modulus along the transverse direction of the fiber
$f(t)$	forcing function
G_{LT}	shear modulus
$[K]$	assembled global stiffness matrix
$[k]$	element stiffness matrix
$[k_{pp}]$	extensional stiffness matrix
$[k_{pf}]$	coupling stiffness matrix
$[k_{ff}]$	bending stiffness matrix
k	layer number
L_1, L_2, L_3	area co-ordinates
$[M]$	assembled global mass matrix
$[m]$	element mass matrix
N	number of layers
$[N]$	shape function matrix for the plate element
$[N_{bm}]$	shape function for 3-D beam element
$[N_p]$, $[N_f]$	in-plane and bending shape functions for plate and shell element
$[Q]$	stress–strain relation matrix in the material co-ordinate
$[\bar{Q}]$	stress–strain relation matrix transformed to the x–y co-ordinate
t	thickness of the laminate
V	volume
$\{u, v, w\}$	nodal displacements
z	layer distance from the mid surface of the laminate
α, β	constants
$\{\delta_p\}$, $\{\delta_f\}$	in-plane and bending nodal displacement vector
$\{\varepsilon\}$	total strain
$\{\varepsilon_p\}$, $\{\varepsilon_f\}$	in-plane and bending strain
θ	fiber angle
$\{\theta_x, \theta_y, \theta_z\}$	nodal rotations for plate elements
$\{\phi, \varphi, \theta\}$	nodal rotations for beam elements
μ_{LT}	the poisson ratio
ρ	density
ω	natural frequency (rad/s)